

# Natural fracture characterization in tight gas sandstones: Integrating mechanics and diagenesis

Jon E. Olson, Stephen E. Laubach, and Robert H. Lander

## ABSTRACT

Accurate predictions of natural fracture flow attributes in sandstones require an understanding of the underlying mechanisms responsible for fracture growth and aperture preservation. Poroelastic stress calculations combined with fracture mechanics criteria show that it is possible to sustain opening-mode fracture growth with sub-lithostatic pore pressure without associated or preemptive shear failure. Crack-seal textures and fracture aperture to length ratios suggest that preserved fracture apertures reflect the loading state that caused propagation. This implies that, for quartz-rich sandstones, the synkinematic cement in the fractures and in the rock mass props fracture apertures open and reduces the possibility of aperture loss on unloading and relaxation. Fracture pattern development caused by subcritical fracture growth for a limited range of strain histories is demonstrated to result in widely disparate fracture pattern geometries. Substantial opening-mode growth can be generated by very small extensional strains (on the order of  $10^{-4}$ ); consequently, fracture arrays are likely to form in the absence of larger scale structures. The effective permeabilities calculated for these low-strain fracture patterns are considerable. To replicate the lower permeabilities that typify tight gas sandstones requires the superimposition of systematic cement filling that preferentially plugs fracture tips and other narrower parts of the fracture pattern.

## INTRODUCTION

The characterization of naturally fractured reservoirs continues to challenge geoscientists. Although a variety of diagnostic techniques depend on the wellbore for data, ranging from conventional fractured

## AUTHORS

JON E. OLSON ~ *Petroleum and Geosystems Engineering, Cockrell School of Engineering, University of Texas at Austin, 1 University Station C0300, Austin, Texas 78712; jolson@mail.utexas.edu*

Jon Olson is an associate professor in the Department of Petroleum and Geosystems Engineering. He joined the faculty in 1995. He has six years of industrial experience. He specializes in the applications of rock fracture and continuum mechanics to fractured reservoir characterization, hydraulic fracturing, and reservoir geomechanics. He was a distinguished lecturer for AAPG in 2007–2008.

STEPHEN E. LAUBACH ~ *Bureau of Economic Geology, John A. and Katherine G. Jackson School of Geosciences, University of Texas at Austin, Austin, Texas 78713-8924; steve.laubach@beg.utexas.edu*

Steve Laubach is a senior research scientist at the Bureau Economic Geology where he conducts research on unconventional and fractured reservoirs. His interests include fluid inclusion and cathodoluminescence studies and application of borehole-imaging geophysical logs to stress and fracture evaluation. He was a distinguished lecturer for the Society of Petroleum Engineers in 2003–2004.

ROBERT H. LANDER ~ *Geocosm LLC, 3311 San Mateo Drive, Austin, Texas 78738; roblander@geocosm.net*

Rob Lander develops diagenetic models for Geocosm LLC. He obtained his Ph.D. in geology from the University of Illinois in 1991, was a research geologist at Exxon Production Research from 1991 to 1993, and worked for Rogaland Research and Geologica AS from 1993 to 2000. He is also a research fellow at the Bureau of Economic Geology.

## ACKNOWLEDGEMENTS

Our research on structural diagenesis is supported by the Chemical Sciences, Geosciences and Biosciences Division, Office of Basic Energy Sciences, Office of Science, U.S. Department of Energy grant DE-FG02-03ER15430 (Predicting fracture porosity evolution in sandstone), by industrial associates of the Fracture Research and Application Consortium and by Geocosm's Consortium for Quantitative Prediction of Sandstone Reservoir Quality. We are grateful to L. M. Bonnell for discussion and to Tricia F. Allwardt and Laird B. Thompson for reviews. The AAPG Editor thanks the following reviewers for their work on this paper: Tricia F. Allwardt and Laird B. Thompson.

Copyright ©2009. The American Association of Petroleum Geologists. All rights reserved.

Manuscript received June 9, 2009; provisional acceptance July 21, 2009; revised manuscript received August 4, 2009; final acceptance August 11, 2009.

DOI:10.1306/08110909100

core description (Nelson, 1985) to the use of microfractures observed in thin sections from core (Laubach, 1997; Laubach and Gale, 2006) to the imaging of large fractures with resistivity or acoustic image logs (Zemanek et al., 1970; Asquith and Krygowski, 2004; Barton et al., 2009, this issue), wellbore fracture observations are by their nature incomplete and, for some key attributes such as fracture length distribution, inadequate (Wu and Pollard, 2002). Geophysical techniques, which infer fracture attributes from their effects on wave propagation, sample a larger volume but have limited capability for unambiguously delineating fractures (e.g., Sayers, 2007). Outcrop analogs are opportunities to make more complete observations of fracture network geometry in at least two dimensions (e.g., Hennings et al., 2000; Laubach and Ward, 2006) but require extrapolating results to subsurface structural and diagenetic conditions. In some cases, quantifying the stress state (magnitudes and directions) is used as a proxy for fracture observations, with the assumption that opening-mode fractures parallel to  $S_{Hmax}$  (the most compressive horizontal stress) are most likely to be conductive (Heffer and Lean, 1993), or faults that are critically stressed are the key to reservoir deliverability (Barton et al., 1995), but this is apparently not generally the case for tight gas sandstones, where open and conductive fractures are found at a wide range of angles to  $S_{Hmax}$  (Laubach et al., 2004a).

Using data collected typically from wellbores or outcrops, geostatistical models, and mechanical stratigraphy are widely employed to infer fracture network attributes away from the wellbore (Datta-Gupta et al., 1995; Ortega et al., 2006; Laubach et al., 2009, this issue; McLennan et al., 2009, this issue; Zahm and Hennings, 2009, this issue). Interwell fracture geometry can also be predicted using geomechanical models of varying complexity, which are constrained by stress state, preexisting large-scale structures, and rock properties (Camac and Hunt, 2009, this issue; Smart et al., 2009, this issue). Finally, in addition to the mechanically generated fracture porosity creation and flow pathway connectivity, simultaneously acting diagenetic processes modify the flow capability of the fracture network (Laubach, 2003; Philip et al., 2005; Laubach and Diaz-Tushman, 2009).

In this article, we analyze the creation of permeable networks of opening-mode fractures from the perspective of fracture mechanics and the modification of mechanically generated aperture by diagenesis, and how these results are applicable to tight gas sandstones. We look at the pore pressure and strain conditions that

can generate fractures, and how stress states control whether rocks fail in tension or shear. The results show that opening-mode fracturing can occur at pore pressures substantially below the overburden stress magnitude and at very small extensional strains, creating fracture networks with considerable flow capacity and low fracture porosity. This propensity of rocks to fail easily in the tensile mode highlights the challenges of predictive natural fracture characterization. Analyses and observations suggest that fractures may form in response to minor geologic events that would be mostly unnoticed if it were not for the fractures that were left behind. Moreover, whether these fractures remain open, and how their capacity to transmit fluids varies with time depend strongly on the mostly thermally driven precipitation reactions of diagenesis, not necessarily the more readily measured present-day stress state.

## INSIGHTS FROM THE MECHANICS OF FRACTURE

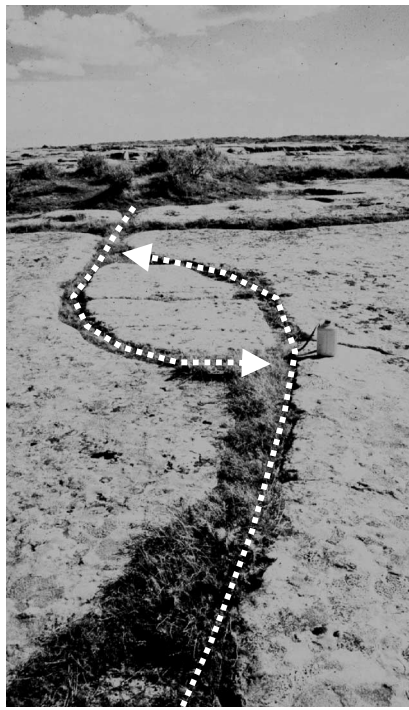
Linear elastic fracture mechanics (LEFM) provide a framework from which fracture propagation can be described as a function of loading, fracture geometry, and material properties (Lawn and Wilshaw, 1975). One key parameter with regard to propagation is the stress intensity factor,  $K_i$  (where  $i = I, II, \text{ or } III$ ), which is a measure of the magnitude of the stress singularity at the crack tip that drives propagation. For pure opening mode (or mode I), the displacement discontinuity across the fracture is normal to the fracture face. Shearing can be describing as mode II sliding (shear is perpendicular to the crack front) or mode III scissoring (shear is parallel to the crack front). Joints and veins are typically a result of mode I or mixed mode I-II or I-III. As described by Pollard and Aydin (1988), pure mode I propagation leads to straight propagation paths (Figure 1a). A combination of mode I and II will result in kinked or curving paths (Olson and Pollard, 1989) (Figure 1b), whereas modes I and III will cause the crack plane to twist or break down into an echelon segments (Pollard et al., 1982) (Figure 1c).

The magnitude of the mode I stress intensity factor for an isolated, uniformly loaded, straight crack under two-dimensional (2-D), plane strain conditions can be written as (Lawn and Wilshaw, 1975)

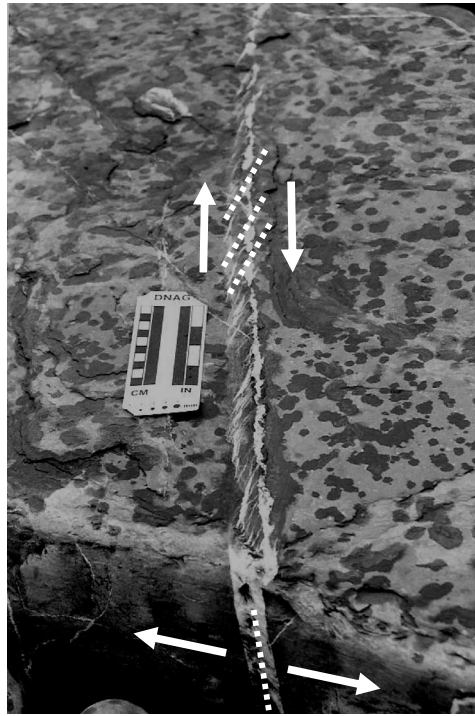
$$K_I = \Delta\sigma_I\sqrt{\pi a} \quad (1)$$



a)



b)



c)

**Figure 1.** Examples of typical fracture propagation modes for joints and veins. (a) Straight fracture geometry indication of pure mode I propagation sandstone, Muddy Gap, Wyoming. (b) Mixed mode I-II curving pattern for overlapping en echelon fractures in sandstone, Oil Mountain, Wyoming. (c) Mixed mode I-III parent crack and en echelon fringe cracks in limestone, Bristol Channel, England. Dotted lines indicate representative fracture planes (a–c), and solid arrows indicate inferred loading conditions (c: opening and right-lateral shear).

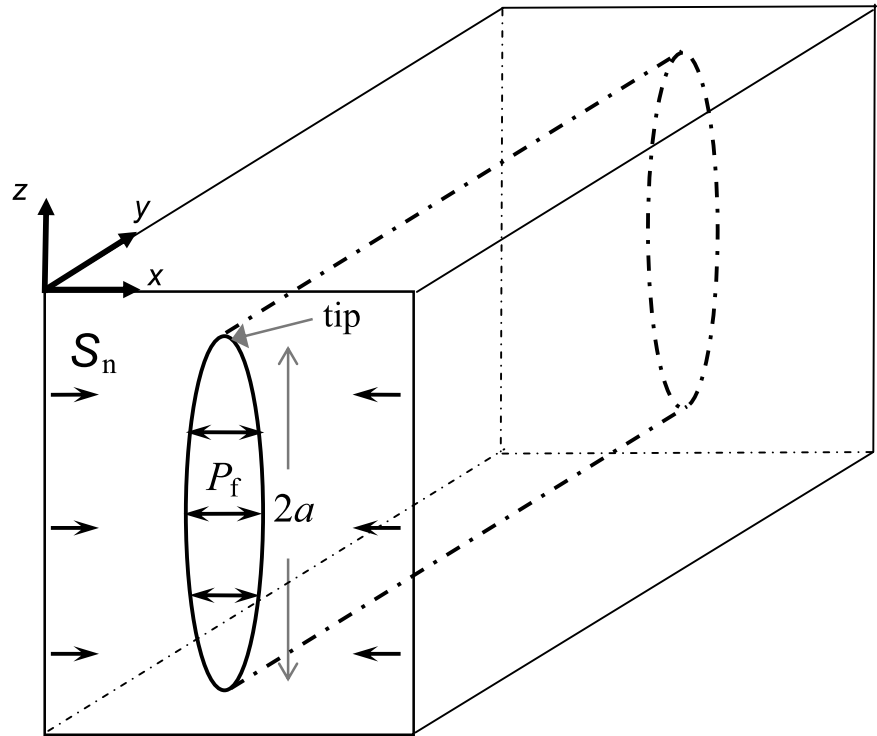
where  $\Delta\sigma_I$  is called the mode I driving stress, given by (Olson, 2003)

$$\Delta\sigma_I = (P_f - S_n) \quad (2)$$

where  $P_f$  is the fluid pressure acting inside the crack,  $S_n$  is the normal stress acting perpendicular to the crack plane (compression assumed positive), and  $2a$  is the dimension of the crack in the plane of analysis (the  $x$ - $z$  plane, Figure 2). Because it is expected that the remote princi-

pal stresses are all compressive in the subsurface (Zoback, 2007), the fluid pressure in the fracture,  $P_f$ , must be greater than  $S_n$  to generate a positive opening-mode driving stress (Segall, 1984). Engelder and Lacazette (1990), in describing the concept of natural hydraulic fracturing, showed that over long periods in a porous media, the fluid pressure in the fracture could be equated with the pore pressure of the formation,  $P_f = P_p$ . Opening-mode fractures typically propagate as planes perpendicular to the least compressive principal stress,  $S_3$  (Lawn and Wilshaw, 1975; Pollard and Aydin, 1988). Vertical

**Figure 2.** Plane strain fracture idealization for analysis in the  $x$ - $z$  plane, showing fracture orientation relative to the coordinate system. Mode I driving stress,  $\Delta\sigma_I$ , for fracture opening and growth is a function of the internal fluid pressure in the fracture,  $P_f$ , and the normal stress acting perpendicular to the fracture plane,  $S_n$ . For vertical fractures, typically  $S_n = S_{hmin}$  ( $S_{hmin}$  is the minimum horizontal compressive stress).



opening-mode fractures consequently imply  $S_n = S_3 = S_{hmin}$  (where  $S_{hmin}$  is the least compressive horizontal stress) indicative of normal faulting ( $S_{vert} > S_{Hmax} > S_{hmin}$ ) or strike-slip faulting ( $S_{Hmax} > S_{vert} > S_{hmin}$ ) stress regimes (where  $S_{vert}$  is the vertical stress). Propagation directions can vary from this simple relationship because of local stress heterogeneities caused by crack to crack interaction (Gross, 1993; Bai et al., 2002; Olson, 2007), stress perturbation caused by fault slip (Rawnsley et al., 1992), or other geologic structures and heterogeneities of local influence.

Crack propagation can be divided into critical and subcritical regimes based on the magnitude of the stress intensity factor,  $K_I$ , relative to fracture toughness,  $K_{Ic}$ . Critical (commonly termed dynamic) propagation occurs when  $K_I \geq K_{Ic}$ , and under sustained loading, propagation will accelerate to rupture velocity, kinetic energy effects become significant, and crack-tip branching may occur (Lawn and Wilshaw, 1975). Subcritical growth occurs at stress intensity factors below fracture toughness,  $K_I < K_{Ic}$ , aided by the action of corrosive fluids that reduce the fracture strength of the material (Anderson and Grew, 1977). Subcritical fracture propagation typically runs at velocities less than  $10^{-3}$  m/s and can be treated as quasi-static, kinetic energy effects being negligible (Segall and Pollard, 1983). A minimum threshold value of the stress intensity factor is required for the

propagation (termed  $K_{Ic}^*$ ), which is estimated to be on the order of  $K_{Ic}^* \cong K_{Ic}/10$  (Segall and Pollard, 1983; Segall, 1984; Atkinson and Meredith, 1987).

Joint and vein networks are widely proposed to represent the result of subcritical fracture growth (Atkinson, 1984; Segall, 1984; Atkinson and Meredith, 1987; Olson, 1993). Given the idea that crack propagation occurs when a threshold value of the stress intensity factor has been reached or exceeded, we can set the stress intensity factor in equation 1 to  $K_I = K_{Ic}^*$  as a condition for subcritical growth, and rearrange the terms to show the driving stress required for propagation of an isolated fracture as (Olson, 2003)

$$\Delta\sigma_I = \frac{K_{Ic}^*}{\sqrt{\pi a}} \quad (3)$$

Segall (1984) proposed that the positive driving stress needed to generate regional opening-mode (joint) patterns can be a result of regional extension imposed on the rock body, widely distributed elevated fluid pressure, or both. Olson (2003) discussed the variation in driving stress under regional extension loading or fluid-pressure-driven natural hydraulic fracturing, arguing that square-root scaling of aperture to length measured in some joints and dikes indicates propagation at constant stress intensity factor.

## FAILURE CONDITIONS IN A POROELASTIC MEDIUM

### Pore-Pressure Conditions for Opening-Mode Growth

The initiation of opening-mode growth for vertical joints or veins in the subsurface requires  $P_p > S_{hmin}$ , and there has been some question as to the likelihood of such conditions (Lorenz et al., 1991). We examine one aspect of this question from the perspective of natural hydraulic fracturing (Engelder and Lacazette, 1990) to illustrate how a porous media can move from stress conditions that inhibit opening-mode fracture growth ( $P_p < S_{hmin}$ ) to conditions that favor it ( $P_p > S_{hmin}$ ). Evidence from subsurface oil and gas operations demonstrates that horizontal in-situ stress varies proportional to pore-pressure change (Lorenz et al., 1991; Engelder and Fisher, 1994). However, field data from the Vicksburg Formation of south Texas (Salz, 1977) illustrate that horizontal stress change is only a fraction of the pore-pressure change ( $\Delta S_{hmin} \cong 0.6\Delta P_p$ ). Similar results are found in other oil and gas fields around the world (Engelder and Fisher, 1994; Segall and Fitzgerald, 1998; Zoback and Zinke, 2002). The proportionality between stress and pore-pressure change has been explained by analyzing the reservoir as a poroelastic solid (Engelder and Fisher, 1994; Segall and Fitzgerald, 1998). As such, the relationship between  $S_{hmin}$  and  $P_p$  should take the form of

$$S_{hmin} = S_{hmin}^0 + \frac{1-2\nu}{1-\nu} \alpha_p P_p \quad (4)$$

where  $\nu$  is Poisson's ratio,  $\alpha_p$  is Biot's poroelastic constant, and  $S_{hmin}^0$  is the part of the horizontal stress that is not pore pressure dependent. The  $S_{hmin}^0$  can be quantified based on plane strain elastic equations as (Prats, 1981; Blanton and Olson, 1999)

$$S_{hmin}^0 = \frac{\nu}{1-\nu} S_{vert} + \frac{E}{1-\nu^2} \epsilon_{tect} + \frac{E}{1-\nu} \alpha_T \Delta T \quad (5)$$

where  $E$  is Young's modulus,  $\epsilon_{tect}$  is the horizontal tectonic strain (used as a calibration term and assumed to be uniform with depth),  $\alpha_T$  is the linear elastic thermal expansion coefficient of the rock, and  $\Delta T$  is the increase in temperature the rock experienced during burial. Other authors have included more complicated earth rheologies such as viscoelasticity to represent the time-dependent deformation expected in rocks over long periods (Narr and Currie, 1982; Warpinski, 1989). We employ this

simpler approach here because we are only interested in pore-pressure effects and because practical application suggests that equations 4 and 5 can be used to adequately represent layer to layer variations in present-day stress for sedimentary sequences (Blanton and Olson, 1999).

Taking the derivative of  $S_{hmin}$  with respect to pore pressure gives

$$\frac{dS_{hmin}}{dP_p} = \frac{1-2\nu}{1-\nu} \alpha_p \quad (6)$$

and using reasonable values for the elastic constants ( $0 < \nu < 0.5$  and  $0 < \alpha_p < 1$ ), we can show that the variation in total horizontal stress with pore pressure ( $dS_{hmin}/dP_p$ ) should always be less than or equal to 1 (Engelder and Fisher, 1994). The ratio of 0.6 observed in the field by Salz (1977) can be obtained with typical sandstone constants of  $\nu = 0.2$  and  $\alpha_p = 0.8$ , among other combinations. Also note that, for pore-pressure change in a laterally extensive permeable zone, the magnitude of the overburden stress ( $S_{vert}$ ) is unaffected (Segall and Fitzgerald, 1998).

The pore pressure required to generate opening-mode fractures can be related to the vertical stress by combining the horizontal stress relations and fracture mechanics equations. Following the conceptual model of Engelder and Lacazette (1990), we combine equations 2 and 3, setting  $S_n = S_{hmin}$  and  $P_f = P_p$ , to find the pore pressure required for the propagation of vertical fractures

$$P_p = S_{hmin} + \frac{K_{Ic}^*}{\sqrt{\pi a}} \quad (7)$$

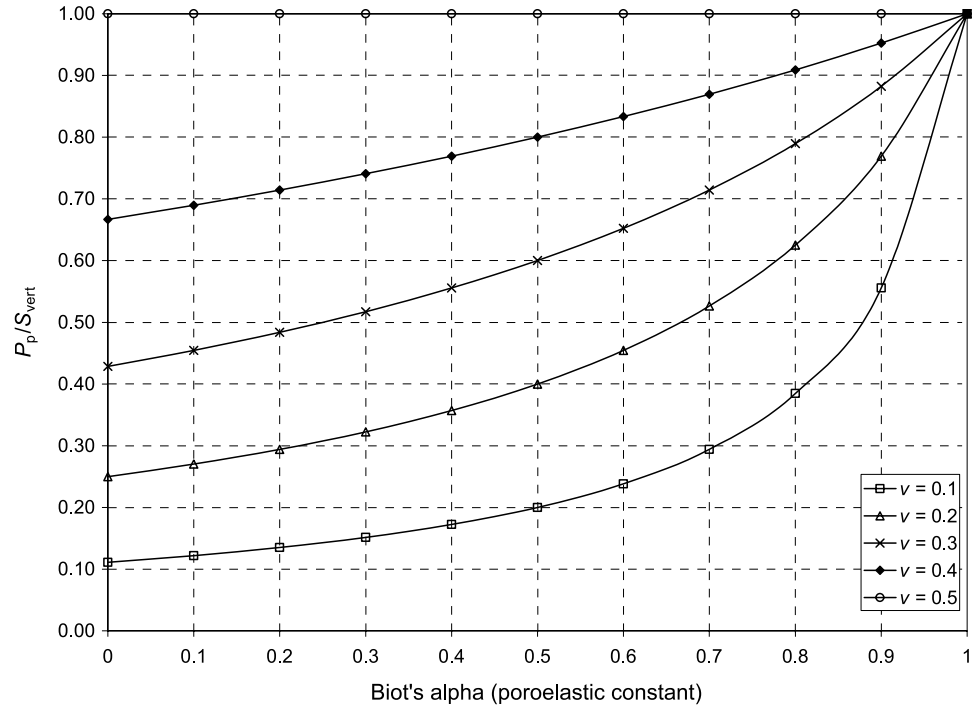
Substituting equation 4 for  $S_{hmin}$  into equation 7 and solving for pore pressure gives an LEFM-poroelastic-based expression for the conditions of opening-mode fracture growth

$$P_p = \frac{(1-\nu)}{(1-\nu - (1-2\nu)\alpha_p)} \left[ S_{hmin}^0 + \frac{K_{Ic}^*}{\sqrt{\pi a}} \right] \quad (8)$$

Expanding the  $S_{hmin}^0$  term and normalizing both sides of equation 8 by the vertical stress,  $S_{vert}$ , gives the ratio of pore pressure to vertical stress for fracture propagation

$$\begin{aligned} P_p/S_{vert} &= \frac{\nu}{(1-\nu - (1-2\nu)\alpha_p)} \\ &+ \frac{1}{S_{vert}} \times \left[ \frac{(1-\nu)}{(1-\nu - (1-2\nu)\alpha_p)} \right] \\ &\times \left[ \frac{E\epsilon_{tect}}{(1-\nu^2)} + \frac{E\alpha_T\Delta T}{(1-\nu)} + \frac{K_{Ic}^*}{\sqrt{\pi a}} \right] \end{aligned} \quad (9)$$

**Figure 3.** Ratio of pore pressure to vertical stress ( $\lambda_p = P_p/S_{\text{vert}}$ ) required for opening-mode fracture growth as a function of Biot's poroelastic parameter,  $\alpha_p$ , and Poisson's ratio,  $\nu$ .



For the sake of discussion, we make a first-order approximation that the tectonic strain and thermoelastic and threshold subcritical stress-intensity terms in equation 9 are small relative to the vertical stress and are thus of only secondary interest. This leaves us with a simpler expression that is useful for estimating the order of magnitude of pore pressure relative to vertical stress required for opening-mode fracturing as

$$P_p/S_{\text{vert}} \cong \frac{\nu}{(1 - \nu - (1 - 2\nu)\alpha_p)} \quad (10)$$

Interestingly, when  $\alpha_p = 1$ , equation 10 becomes independent of Poisson's ratio and is always equal to 1 (Figure 3). However, when  $\alpha_p < 1$ , the pore-pressure ratio required for fracturing can drop to below hydrostatic ( $P_p/S_{\text{vert}} \cong 0.4$ ) depending on the value of Poisson's ratio. The better the cement and the lower the porosity in a sandstone, the lower its poroelastic constant is expected to be. Consequently, for such rocks, the first-order approximation of equation 10 suggests that opening-mode fracturing can occur at pore pressures significantly less than the overburden stress, and given typical elastic values for tight gas sandstones ( $\nu < 0.3$  and  $0.5 < \alpha_p < 0.7$ ), even subhydrostatic pore pressure could be conducive to opening-mode failure (Figure 3).

### Shear Failure Versus Tensile Failure

One last factor to consider when looking at the likelihood of natural hydraulic fracturing is whether the layer will fail in shear before the tensile failure criterion is met. Because shear failure also becomes more likely when the pore pressure reaches a significant fraction of the vertical stress and fault slip can relieve driving stresses that may also cause opening-mode failure, it seems probable that if the shear failure occurs first on a typical loading path, it will suppress or possibly prevent later opening-mode failure. We test this concept using a simple Mohr-Coulomb shear failure criterion (Jaeger and Cook, 1979). Zoback and Healy (1984) showed that the Mohr-Coulomb frictional sliding on preexisting faults is a reasonable model for constraining in-situ stress magnitudes on a regional scale. For our purposes, we are interested in stresses at the well scale or outcrop scale in a bed of intact rock (no preexisting faults), and we want to see if that particular layer will fail first in shear or tension. Stability with respect to Mohr-Coulomb failure can be described as (Zoback, 2007)

$$(S_1 - P_p) < \left( \sqrt{1 + \mu_i^2} + \mu_i \right)^2 (S_3 - P_p) + \text{UCS} \quad (11)$$

**Table 1.** Mechanical Property and In-Situ Stress Data for Canyon Group, Sonora Gas Field, Texas

Depth (m)	Lith**	$S_{\text{vert}}$ (MPa)	$E$ (GPa)	$\nu$	$\alpha_p$	$P_p$ (MPa)	$\alpha_T$	$\Delta T$ (°F)	$S_{\text{hmin}}^*$ (MPa)	$S_{\text{hmin}}$ (MPa)
1844	ss	45.5	46.9	0.23	0.59	13.8	$5.6 \times 10^{-6}$	90.8	31.2	29.6
941	ss	47.9	53.8	0.15	0.63	14.5	$5.6 \times 10^{-6}$	95.5	26.8	27.4
1954	sh	48.2	32.4	0.30	0.62	14.6	$5.0 \times 10^{-6}$	96.2	33.5	33.2
1987	ss	49.0	55.2	0.13	0.64	14.8	$5.6 \times 10^{-6}$	97.8	27.5	27.3
2002	sh	49.4	32.4	0.29	0.63	14.9	$5.0 \times 10^{-6}$	98.5	33.2	34.0
2017	ss	49.7	51.7	0.15	0.64	15.1	$5.6 \times 10^{-6}$	99.3	28.1	29.1
2045	sh	50.4	27.6	0.30	0.67	15.3	$5.0 \times 10^{-6}$	100.6	35.6	35.1

\*\*Lith = lithology; ss = sandstone; sh = shale.

where  $S_1$  and  $S_3$  are the most and least compressive principal stresses, respectively,  $\mu_i$  is the coefficient of internal friction, and UCS is the unconfined compressive strength. If the inequality of equation 11 is true, Mohr-Coulomb shear failure should not occur. To determine if opening-mode failure will occur at a pore pressure lower than that required for shear failure (i.e., opening-mode failure will occur first), we can substitute the pore-pressure value  $P_p = S_3$  into equation 11, which is our nominal condition for opening-mode growth. The term  $(S_3 - P_p)$  then becomes zero, and equation 11 can be rewritten as

$$S_3/S_1 > 1 - \text{UCS}/S_1 \quad (12)$$

or noting that  $P_p$  and  $S_3$  are interchangeable

$$P_p/S_1 > 1 - \text{UCS}/S_1 \quad (13)$$

If this condition is true, then opening-mode failure is likely to precede shear failure. This is a useful result in that it only depends on one rock property, unconfined compressive strength (UCS). If we assume a normal faulting stress regime ( $S_1 = S_{\text{vert}}$ ), we can rewrite equation 13 in terms of the vertical stress (to be analogous to equations 9 and 10) as

$$P_p/S_{\text{vert}} > 1 - \text{UCS}/S_{\text{vert}} \quad (14)$$

### SONORA FIELD, CANYON GROUP EXAMPLE

In summary, we have defined a possible set of constraints on pore pressure for the generation of vertical, opening-mode fractures. A quantitative example, based on measured subsurface data from the Philips C-11 Ward well in the Canyon Group of the Sonora field, Texas (Miller et al., 1994), illustrates how this ap-

proach can be applied to fracture prediction. At the time of the stress measurements, the Sonora Canyon reservoir was underpressured ( $dP_p/dz = 7.6$  MPa/km) and  $P_p < S_{\text{hmin}}$ . Table 1 summarizes the in-situ data collected for this well in each of seven zones, including the magnitude of the least compressive horizontal stress as measured by microfractures (labeled  $S_{\text{hmin}}^*$ ). The last column in Table 1 (labeled  $S_{\text{hmin}}$ ) is the best estimate of the least compressive horizontal stress applying equations 4 and 5 with a tectonic strain value of  $\epsilon_{\text{tect}} = -4.017 \times 10^{-4}$ .

The pore-pressure ratio,  $\lambda_p = P_p/S_{\text{vert}}$ , to satisfy the nominal opening-mode fracturing condition of  $P_p = S_{\text{hmin}}$ , was computed using equation 9 (Table 2). We again assumed that  $(K_{\text{lc}}^*/\sqrt{\pi a})S_{\text{vert}} \ll 1$  and could be neglected, but we did include the tectonic and thermal strain terms as constrained by the stress analysis of Table 1. The pore-pressure ratios required to initiate opening-mode fracturing for the seven zones in the Sonora field Canyon Group represent significant overpressures, ranging from  $\lambda_p = 0.86$  to  $\lambda_p = 0.94$ , but the pore pressures are all below the overburden stress. The calculations also predict that natural hydraulic fracturing

**Table 2.** Predicted Failure Data for Sonora Gas Field

Depth (m)	Lith*	$\lambda_p$	UCS (MPa)	$1 - \text{UCS}/S_{\text{vert}}$	$1 - (\text{UCS}/10)/S_{\text{vert}}$
1844	ss	0.90	149	-2.28	0.67
1941	ss	0.86	180	-2.76	0.62
1954	sh	0.91	86	-0.78	0.82
1987	ss	0.86	187	-2.81	0.62
2002	sh	0.92	86	-0.74	0.83
2017	ss	0.90	170	-2.42	0.66
2045	sh	0.94	77	-0.52	0.85

\*Lith = lithology; ss = sandstone; sh = shale.

would occur at lower pore-pressure ratios in the stronger sandstones than in the weaker shales, although the difference is slight.

Using equation 14, we tested whether opening-mode failure was likely to precede shear failure. The UCS values were estimated using a Young's modulus correlation from Zoback (2007, his tables 4.1 and 4.2). Given the very high estimated UCS values (70 MPa or higher), the quantity  $(1 - UCS/S_{vert})$  was negative for all depths (Table 2), clearly satisfying the inequality in equation 14 and indicating that opening-mode fracturing would occur before faulting. We also tried 1/10 of the UCS values from the correlations for each zone to see if reducing rock strength would significantly change the result. All zones still passed the test that opening-mode fracture initiation would precede faulting, but the margin of difference was much smaller (Table 2). Core observations from other wells in the Sonora Canyon reveal porous, quartz-bridged opening-mode fractures (Laubach et al., 2009, this issue), which is consistent with the model prediction.

## FRACTURE PROPAGATION MODELING

Given the premise that opening-mode fracture growth can be driven by reasonable combinations of tectonic strain and pore pressure, we employ the joints model described by Olson (2004, 2007) to investigate fracture porosity and permeability generation under small strain loading. The numerical model simulates lateral propagation of vertical fractures in a semi-infinite elastic media where the fractures are confined to a horizontal, finite thickness layer (see Olson, 2003, 2004, for a detailed discussion of the three-dimensional aspects of the modeling). Accounting for the stress shadow effects of finite height fractures in bedded sedimentary sequences is essential in explaining the common correlation between fracture spacing and layer thickness (Narr and Suppe, 1991; Bai and Pollard, 2000).

Propagation is assumed to be subcritical, whereby propagation velocity can be described as a direct function of stress intensity factor (Atkinson, 1987) as

$$V = A(K_I/K_{Ic})^n \quad (15)$$

where  $A$  is the velocity constant and the exponent  $n$  is called the subcritical index, both empirically determined. For tests done in air, the lowest values of the subcritical index are found for silica glass ( $n \cong 15$ ) and weakly cemented sandstone ( $n \cong 25$ ), whereas the high-

**Table 3.** Modeling Parameters for Fracture Pattern Generation

Finite body, areal extent	$7.2 \times 7.2$ m
Fracture propagation area	$6 \times 6$ m
Layer thickness	1 m
Fracture toughness, $K_{Ic}$	1.5 MPa- $\sqrt{m}$
Young's modulus	20 GPa
Poisson's ratio	0.2
Friction coefficient	0.6
Subcritical index	50
Initial flaw length	0.1 m
Number of flaws	100

est values are obtained for carbonates and shales ( $n > 100$ ) (Atkinson, 1987; Holder et al., 2001). Typical values for well-cemented sandstones fall in the range of  $40 \leq n \leq 80$  in air and water (Rijken et al., 2002; Rijken, 2005). We chose an average value of  $n = 50$  for the simulations presented below.

Three simulations were performed to examine the influence of strain anisotropy on fracture growth driven from flaws under constant pore pressure with initial conditions such that  $P_p = S_{hmin} = S_{yy}$ . The mechanical properties and geometry of the fracturing layer are summarized in Table 3. Figure 4a–c are trace maps illustrating the diversity of fracture pattern geometry that results for even a minor loading path variation. Figure 4d–f are depictions of the aperture distributions for the three different simulations. In all three cases, the fractures propagated from 100 initial flaws of 0.1 m (0.3 ft) total length in response to a biaxial strain of  $\epsilon_{xx} = \epsilon_{yy} = 2 \times 10^{-4}$  imposed in 20 equal increments over 10 m.y., resulting in an effective strain rate of  $\partial\epsilon/\partial t = 6.3 \times 10^{-19}/s$ . All fracture elements had a length of 0.05 mm (0.001 in.), and fracture growth was achieved by adding elements at the crack tips proportional to the propagation velocity calculated using equation 15 (see Olson, 2007, for details on the propagation algorithm). The fracture geometry results ranged from a random polygonal pattern (Figure 4a, d) to a cross-fractured pattern (Figure 4b, e) to a single set of nominally parallel fractures (Figure 4c, f). The difference between the three simulations was achieved by varying the anisotropy of the initial horizontal strains applied to the layer. The initial strain in the  $y$  direction was zero for all three cases ( $\epsilon_{yy} = 0$ ), but the initial strain in the  $x$  direction was varied from  $\epsilon_{xx} = 0$  (Figure 4a, d) to  $\epsilon_{xx} = -1 \times 10^{-4}$  (Figure 4b, e) to  $\epsilon_{xx} = -2 \times 10^{-4}$  (Figure 4c, f), representing an increasing anisotropy

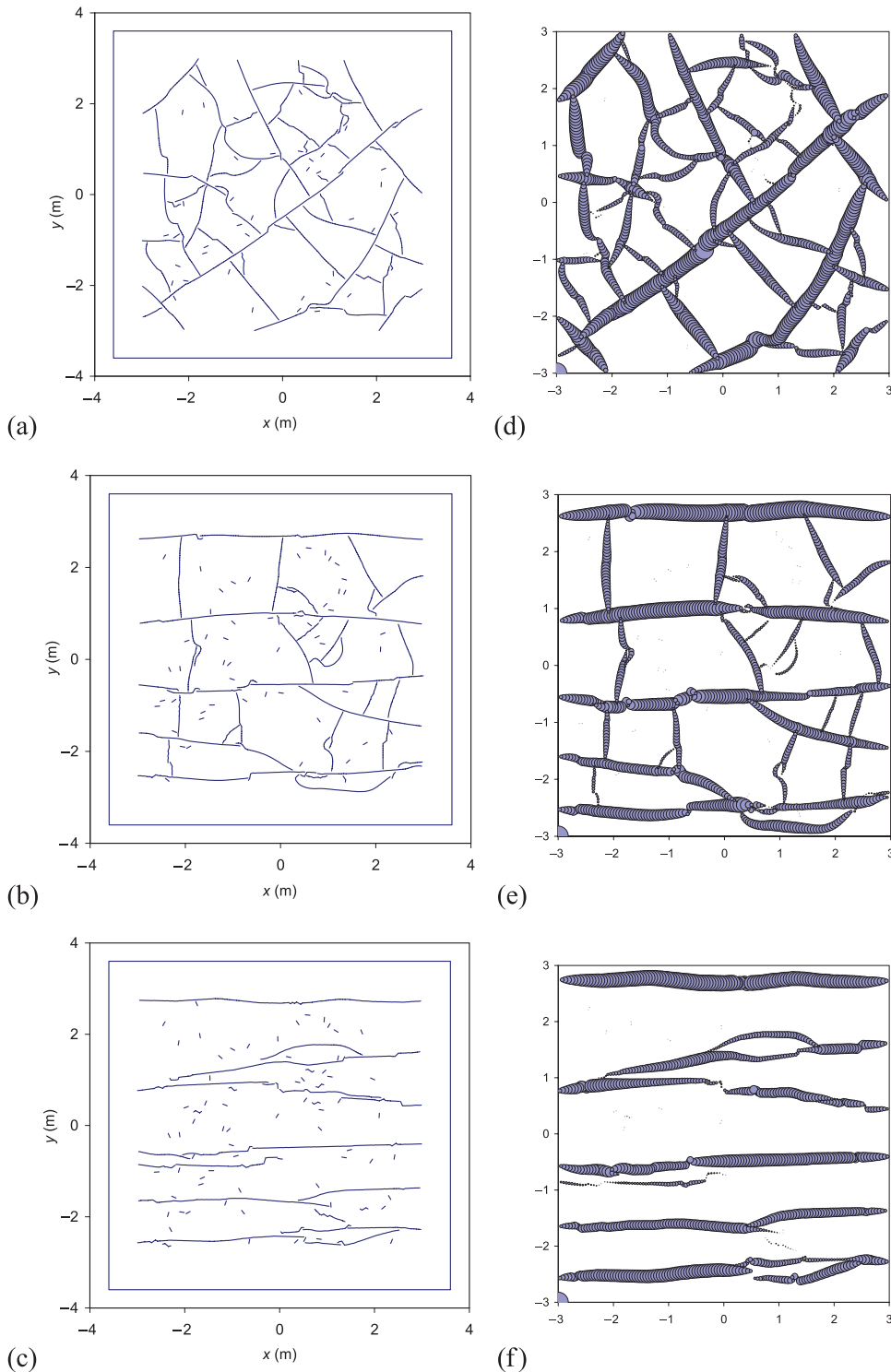


**Figure 4.** Networks of vertical fractures generated from 100 starter flaws in a semi-infinite elastic body with areal ( $x, y$ ) dimensions of 7.2 by 7.2 m (23.6 by 23.6 ft) (areal boundaries indicated by solid-lined squares outlining fracture patterns in panels a–c). Fractures are limited to grow within a 6 by 6 m (20 by 20 ft) window to minimize edge effects (see Olson, 1993). Fractures have a fixed height of 1 m (3 ft) as if constrained to a finite thickness layer, but the body has infinite thickness in the  $z$  direction. (a–c) Trace maps and (d–f) aperture distributions are plotted for three different cases of initial strain anisotropy: (a, d) isotropic initial strain, (b, e) initial  $x$ -parallel contraction strain of  $\epsilon_{xx} = -1 \times 10^{-4}$ , and (c, f) initial strain  $\epsilon_{xx} = -2 \times 10^{-4}$ . Aperture distributions (d–f) are plotted using circles centered on each fracture element with a diameter equal to aperture (diameter of quarter circle in the lower left of each diagram for scale, representing an opening of  $1 \times 10^{-3}$  m [ $3 \times 10^{-3}$  m], exaggeration about 150 times). See Table 3 for additional parameters.

with  $S_{xx}$  being more compressive than  $S_{yy}$ . This increasing stress anisotropy progressively inhibited fracture curving and reorientation away from the  $x$  direction (also the  $S_{Hmax}$  direction), a phenomenon reflecting the competition between in-situ stress and mechanical crack interaction in controlling fracture propagation paths

(Olson and Pollard, 1989). The results suggest that very small variations in the strain state (on the order of  $10^{-4}$  strain) can significantly alter the fracture pattern geometry.

These numerically generated fracture patterns also illustrate that extensive opening-mode fracture patterns can be generated with very small incremental strains, on

the order of  $10^{-4}$ , strains that would probably be undetectable if not for the fracture patterns they left behind. The model prediction of substantial fracture growth at small strain is consistent with field-measured fracture strains on the order of  $10^{-4}$  for closely spaced, mineralized joints in granite (Segall and Pollard, 1983) and with small fracture strain values measured from tight gas sandstones (Hooker et al., 2009).

## EFFECTIVE PERMEABILITY AND DIAGENESIS

Another challenge for fractured reservoir characterization is quantifying the effective permeability of fracture networks like those in Figure 4 (Table 4). A benefit of the mechanics-based analysis exemplified above is that fracture aperture is an intrinsic part of the solution; a result of boundary conditions imposed, propagation criteria, and the mechanical interaction between neighboring fractures. To demonstrate the influence of fracture pattern variability on flow properties, we can quantify the effective permeabilities in the  $x$  and  $y$  directions,  $k_x$  and  $k_y$ , using a finite difference solution that accounts for contributions from both the matrix and fractures (Philip et al., 2005; Olson et al., 2007). The 2-D, steady-state flow equations for an anisotropic, nonhomogeneous media can be written as (Bear, 1979)

$$\frac{\partial}{\partial x} \left( k_x \frac{\partial P}{\partial x} \right) + \frac{\partial}{\partial y} \left( k_y \frac{\partial P}{\partial y} \right) = 0 \quad (16)$$

This equation was solved using the central finite difference method (Bear, 1979) on a 120 by 120 base grid with grid-block (cell) dimensions of  $\Delta x = \Delta y = 0.05$  m (0.01 ft). The flow boundaries were moved in 5% from the edge of the 120 by 120 grid in an attempt

**Table 4.** Simulation Results: Aperture, Fracture Porosity, and Effective Permeability

Pattern	Polygonal	Cross-Fracture	Parallel
Porosity (%)	0.079	0.063	0.052
$k_x$ (md)	8514	5978	4149
$k_y$ (md)	8734	687	0.15
$d_{avg}$ (m)	$3.71 \times 10^{-4}$	$3.46 \times 10^{-4}$	$3.35 \times 10^{-4}$
$d_{max}$ (m)	$9.26 \times 10^{-4}$	$8.85 \times 10^{-4}$	$7.84 \times 10^{-4}$
$d_{min}$ (m)	$1.20 \times 10^{-6}$	$1.35 \times 10^{-6}$	$1.01 \times 10^{-6}$

to avoid the influence of nonsystematic fracture geometry on the edge of the fracture patterns. Because the dimension of the grid blocks was comparable to the fracture element size (0.05 m [0.01 ft]), the flow grid could be readily overlaid on the fracture pattern. Grid blocks that included a fracture element were given a permeability,  $k_{fractd}$ , proportional to the fracture aperture size of the included element, whereas grid blocks without fractures were assigned a matrix permeability value. The permeability of fractured grid blocks was computed as (Philip et al., 2005)

$$k_{fractd} = \frac{k_f \times d + k_m \times (\Delta c - d)}{\Delta c} \quad (17)$$

where  $k_m$  is the matrix permeability ( $k_m = 0.1$  md) and  $k_f$  is the intrinsic fracture permeability

$$k_f = \frac{d^2}{12} \quad (18)$$

The  $\Delta c$  is the grid-block dimension (equivalent to  $\Delta x$  and  $\Delta y$ ), and  $d$  is the fracture aperture. For fractures not aligned with the  $x$  or  $y$  direction, we followed the procedure of Rijken (2005) and introduced off-diagonal grid blocks with fractured block attributes to maintain fracture flow continuity. The permeability of the fractured, fine-scale grid-blocks was assumed to be isotropic ( $k_x = k_y = k_{fractd}$ ). This method was shown to be accurate with respect to analytical steady-state solutions when grid refinement was such that at least four nonfractured grid blocks between parallel fractures were maintained (Philip et al., 2005).

The polygonal fracture pattern (Figure 4d), which was generated under isotropic strain conditions, has a nominally isotropic effective permeability of  $k_x = 8514$  md and  $k_y = 8734$  md. The cross-fractured pattern (Figure 4e), where the apertures for throughgoing fractures parallel to  $x$  are clearly larger than the cross-fractures, has a  $k_x = 5978$  md and  $k_y = 687$  md, a permeability anisotropy of almost 9:1. Finally, the single-set fracture pattern (Figure 4f) has permeabilities of  $k_x = 4149$  md and  $k_y = 0.15$  md. These permeabilities are high for tight gas sandstones, but the calculations presume that all of the mechanically generated apertures for the fracture patterns in Figure 4 are preserved for flow. However, in fractures formed in the subsurface, crack-seal textures and other evidence suggest that cement may be deposited simultaneously with fracture opening and propagation (synkinematic cement), partially filling and propping the large aperture parts of the

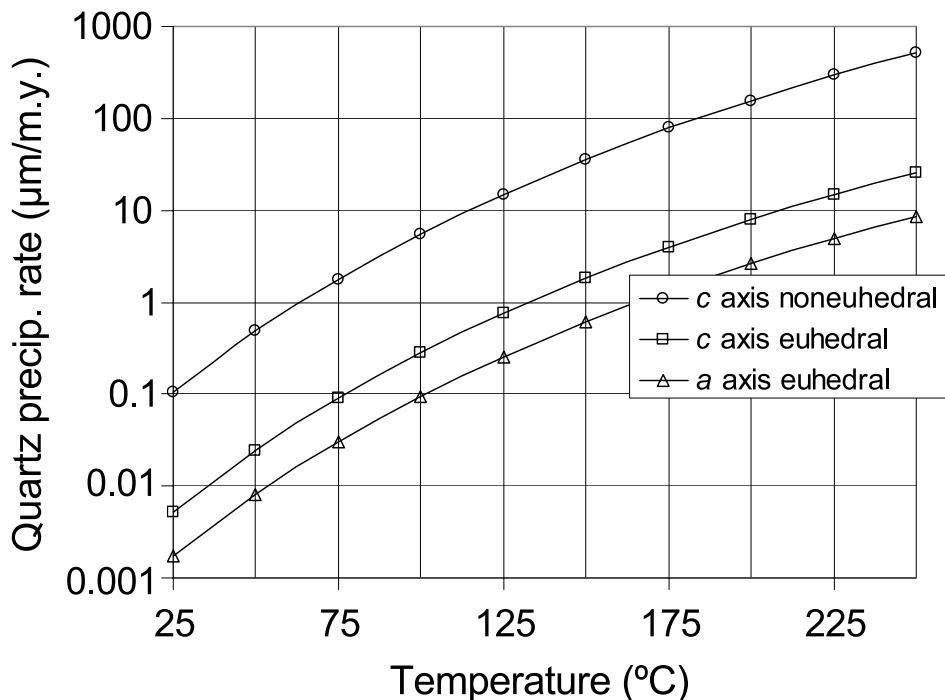


**Figure 5.** Quartz precipitation rate in micrometers per million years for a range of temperature from 25 to 250°C. The three curves represent the range of expected growth rate in a fracture, with the greatest rate being parallel to the *c* crystallographic axis for noneuhedral crystals, followed by *c* axis parallel growth on euhehdral crystals, with the slowest growth parallel to the *a* axis on euhehdral crystals.

fracture pattern but completely plugging and occluding narrower sections such as fracture tips (Laubach, 1988, 2003; Laubach et al., 2004b; Laubach and Ward, 2006; Gale et al., 2009; Hooker et al., 2009). Mapping of quartz cement in fracture bridges, combined with fluid inclusion analysis, suggests that an incremental crack-seal opening for a given fracture may persist for as long as 50 m.y. (Becker et al., in press).

The highly heterogeneous quartz cement thicknesses found in partially cemented fractures are a function of the processes that control quartz crystal growth rates (Lander et al., 2008). Quartz crystals show substantial anisotropies in growth rate depending on the nucleation substrate. The fastest rates of growth occur on noneuhedral surfaces that are perpendicular to the crystallographic *c* axis. Rates are about 20 to 60 times slower, respectively, on euhehdral pyramidal and euhehdral prismatic faces. Quartz growth rate is also a strong function of temperature, which can be expressed using an Arrhenius expression (Walderhaug, 2000; Lander et al., 2008) as

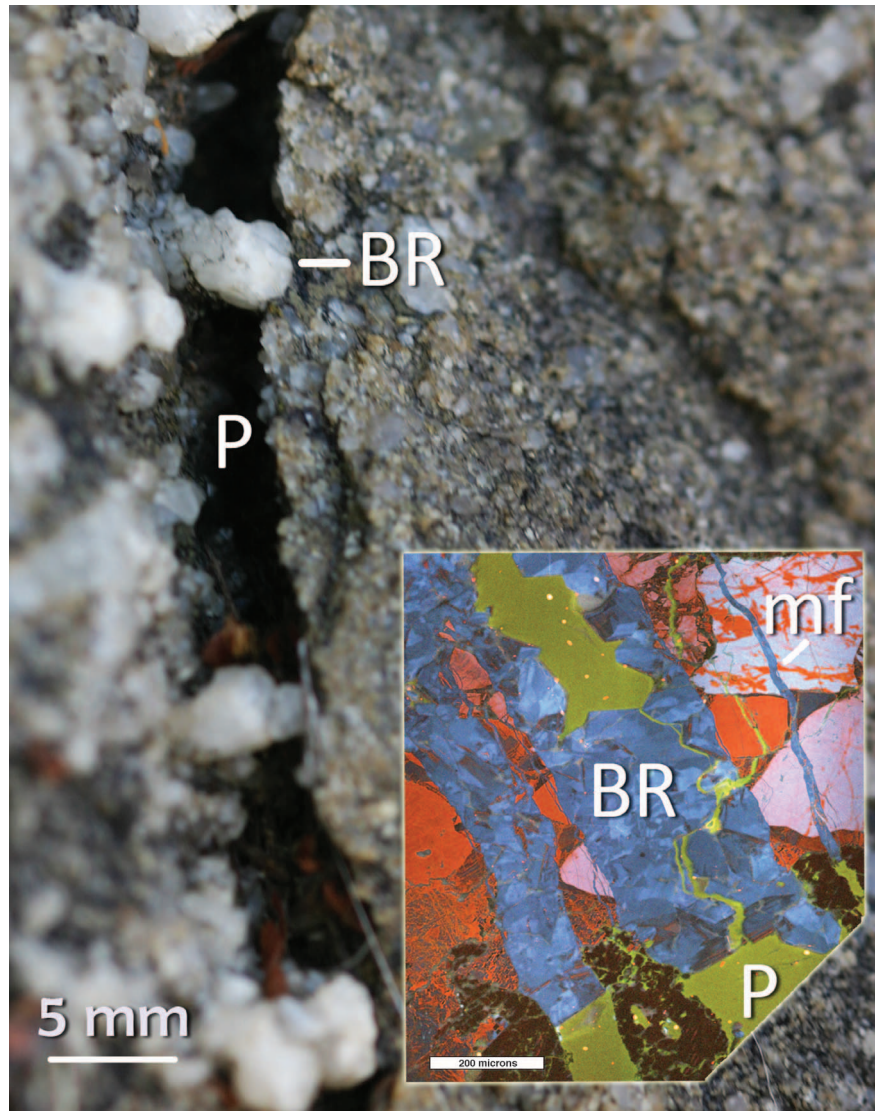
$$q = Ae^{-\frac{Ea_{nc}}{RT}} \quad (19)$$

where  $q$  is the rate of quartz precipitation per unit area ( $\text{mol}/\text{cm}^2\text{s}$ ),  $A$  is a constant ( $\text{mol}/\text{cm}^2\text{s}$ ),  $Ea_{nc}$  is the activation energy for quartz precipitation on noneuhedral *c* axis surfaces ( $\text{J}/\text{mol}$ ),  $R$  is the real gas constant ( $8.314 \text{ J}/\text{mol}^\circ\text{K}$ ), and  $T$  is the temperature (K).

The values in Figure 5 were generated using  $A = 9 \times 10^{-9} \text{ mol}/\text{cm}^2\text{s}$  and  $Ea_{nc} = 49 \text{ kJ}/\text{mol}$ . The latter value was obtained by matching simulated quartz cement abundances to measured values for an unfractured sandstone sample in the Travis Peak Formation using the Prism2D model described by Lander et al. (2008).

The competition between quartz precipitation rate and fracture opening rate determines whether a fracture is completely filled with cement (no porosity), partially filled with occasional aperture spanning bridges that prop it open, or mostly open with only a thin coating of euhehdral quartz crystals (Figure 6). All of these eventualities can be observed in quartz-rich sandstone samples from the subsurface (e.g., Laubach, 2003; Becker et al., in press) and outcrop (Laubach and Ward, 2006; Laubach and Diaz-Tushman, 2009). To estimate the impact of quartz cement precipitation on fracture permeability, we employ the concept of emergent threshold (Laubach, 2003), an empirical observation that, in many quartz-rich sandstones, a kinematic aperture exists below which fractures are completely filled with cement and occluded and above which they are only partially cemented and bridged or completely open. We can estimate the emergent threshold by picking the slowest precipitation rate (parallel to the *a* axis on a euhehdral surface) indicative of the sandstone's temperature during fracturing (Figure 5). Any fracture segment that opened more slowly than this rate should be completely sealed. Fracture segments opening at a

**Figure 6.** Quartz cement bridges crossing open fracture. The inset is the color cathodoluminescence bridge image. BR = bridges; P = porosity. Note the crack-seal texture with quartz grain embedded in bridge quartz cement (blue), porosity, and cement-filled microfracture (mf). Triassic–Jurassic La Boca Formation described by Laubach and Ward (2006).



greater rate but more slowly than the fastest crystal growth rate ( $c$  axis, noneuhedral) should have distributed bridges propping them open. Fracture segments opening faster than the fastest precipitation rate should have only a thin coating of euohedral synkinematic cement.

To demonstrate the effect of synkinematic cement on flow, we recalculated the permeability for the cross-fracture pattern (Figure 4e) for a range of emergent threshold values. The results show that because the through-going and cross-fracture sets have different magnitude apertures (Figure 4e), they suffer drastic permeability reduction at different values of emergent threshold (Figure 7). At an emergent threshold of approximately  $1.4 \times 10^{-4}$  m ( $4.5 \times 10^{-4}$  ft),  $k_y$  drops by two orders of magnitude because the fractures no longer percolate in the  $y$  direction. However, for the throughgoing fractures,

which were better connected initially, percolation in the  $x$  direction is not lost until an emergent threshold of  $2.8 \times 10^{-4}$  m ( $9.1 \times 10^{-4}$  ft), and although permeability drops almost three orders of magnitude, the effective permeability  $k_x$  is still substantially above matrix values (almost a factor of 10). These permeability values incorporating synkinematic cement are more representative of values seen in the field for tight gas sandstones or tight, fractured carbonates (Philip et al., 2005).

## CONCLUSIONS

We have presented a mode of natural fracture analysis that incorporates fracture mechanics and diagenetic processes to predict fracture network geometry and fracture

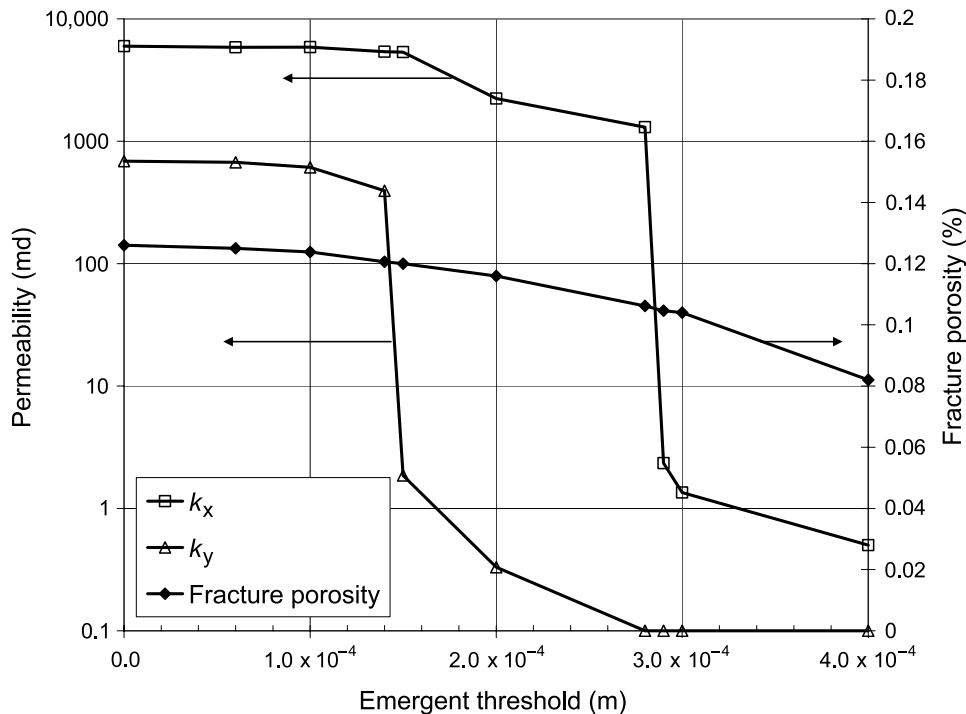


**Figure 7.** Modification of the calculated steady-state effective permeability (left axis) for the fracture pattern of Figure 4e, showing reduction in effective permeabilities,  $k_x$  and  $k_y$ , caused by quartz cementation represented by the increasing emergent threshold. Fracture porosity is plotted on the right axis.

aperture distribution and preservation. Using stress data from a low-permeability gas field in Texas, poroelastic stress calculations combined with fracture mechanics criteria show that it is possible to sustain opening-mode fracture growth with sublithostatic pore pressure without associated or preemptive shear failure. Representative numerical simulations of fracture pattern development caused by subcritical fracture growth demonstrate that substantial opening-mode growth can occur at tiny extensional strains (on the order of  $10^{-4}$ ). The effective permeabilities for these low-strain fracture patterns can be considerable if calculated using the ultimate mechanical opening experienced during propagation, but permeabilities are significantly reduced when accounting for likely diagenetic modifications to the fracture apertures. Significant changes in fracture pattern geometry and flow properties caused by minor changes in deformational or diagenetic boundary conditions highlight the challenges of accurate characterization of natural fractures caused by small strain events. The potential lack of dependence of opening-mode fracture network characteristics on more readily observable macroscopic structures such as folds and faults emphasizes the importance of site-specific subsurface observations of fracture attributes, including diagenesis, that can only be acquired from core. In the absence of subsurface rock samples, wellbore observations via logs and reservoir imaging using geophysical techniques need to be augmented with modeling

predictions constrained by reasonable geologic boundary conditions to assess fracture pattern details that are below observational thresholds.

## REFERENCES CITED

- Anderson, O. L., and P. C. Grew, 1977, Stress corrosion theory of crack propagation with applications to geophysics: *Reviews of Geophysics and Space Physics*, v. 15, p. 77–104.
- Asquith, G., and D. Krygowski, 2004, *Basic well log analysis: AAPG Methods in Exploration Series 16*, 240 p.
- Atkinson, B. K., 1984, Subcritical crack growth in geological materials: *Journal of Geophysical Research*, v. 89, p. 4077–4114, doi:10.1029/JB089iB06p04077.
- Atkinson, B. K., 1987, Introduction to fracture mechanics and its geophysical applications, in B. K. Atkinson, ed., *Fracture mechanics of rock*: London, Academic Press, p. 1–26.
- Atkinson, B. K., and P. G. Meredith, 1987, The theory of subcritical crack growth with applications to minerals and rocks, in B. K. Atkinson, ed., *Fracture mechanics of rock*: London, Academic Press, p. 111–166.
- Bai, T., and D. D. Pollard, 2000, Fracture spacing in layered rocks: A new explanation based on the stress transition: *Journal of Structural Geology*, v. 22, p. 43–57, doi:10.1016/S0191-8141(99)00137-6.
- Bai, T., L. Martin, M. R. Gross, and A. Aydin, 2002, Orthogonal cross joints: Do they imply a regional stress rotation?: *Journal of Structural Geology*, v. 24, p. 77–88, doi:10.1016/S0191-8141(01)00050-5.
- Barton, C., D. Moos, and K. Tezuka, 2009, Geomechanical wellbore imaging: Implications for reservoir fracture permeability: *AAPG Bulletin*, v. 93, no. 11, p. 1551–1569, doi:10.1306/06180909030.

- Barton, C. A., M. D. Zoback, and D. Moos, 1995, Fluid-flow along potentially active faults in crystalline rock: *Geology*, v. 23, p. 683–686, doi:10.1130/0091-7613(1995)023<0683:FFAPAF>2.3.CO;2.
- Bear, J., 1979, *Hydraulics of groundwater*: New York, McGraw-Hill, 567 p.
- Becker, S. P., P. Eichhubl, S. E. Laubach, R. M. Reed, R. H. Lander, and R. J. Bodnar, in press, A 48 m.y. history of fracture opening, Cretaceous Travis Peak Formation, east Texas: *Geological Society of America Bulletin*.
- Blanton, T. L., and J. E. Olson, 1999, Stress magnitudes from logs: Effects of tectonic strains and temperature: *Society of Petroleum Engineers Reservoir Evaluation and Engineering*, v. 2, p. 62–68.
- Camac, B. A., and S. P. Hunt, 2009, Predicting the regional distribution of fracture networks using the distinct element numerical method: *AAPG Bulletin*, v. 93, no. 11, p. 1571–1583, doi:10.1306/07230909040.
- Datta-Gupta, A., L. W. Lake, and G. A. Pope, 1995, Characterizing heterogeneous permeable media with spatial statistics and tracer data using sequential simulated annealing: *Mathematical Geology*, v. 27, p. 763–787, doi:10.1007/BF02273537.
- Engelder, T., and M. P. Fisher, 1994, Influence of poroelastic behavior on the magnitude of minimum horizontal stress,  $S_{h1}$ , in overpressured parts of sedimentary basins: *Geology*, v. 22, p. 949–952, doi:10.1130/0091-7613(1994)022<0949:IOBPOT>2.3.CO;2.
- Engelder, T., and A. Lacazette, 1990, Natural hydraulic fracturing, in N. Barton and O. Stephansson, eds., *Rock joints*: Rotterdam, A. A. Balkema, p. 35–44.
- Gale, J. F. W., R. H. Lander, R. M. Reed, and S. E. Laubach, 2009, Modeling fracture porosity evolution in dolostone: *Journal of Structural Geology*, v. 31, doi:10.1016/j.jsg.2009.04.018.
- Gross, M. R., 1993, The origin and spacing of cross joints: Examples from the Monterey Formation, Santa Barbara coastline, California: *Journal of Structural Geology*, v. 15, p. 737–751, doi:10.1016/0191-8141(93)90059-J.
- Heffer, K. J., and J. Lean, 1993, Earth stress orientation-control on, and guide to, flooding directionality in a majority of reservoirs, in W. Linville, ed., *Reservoir characterization III*: Tulsa, Penn-Well Books, p. 799–822.
- Hennings, P. H., J. E. Olson, and L. B. Thompson, 2000, Combining outcrop and three-dimensional structural modeling to characterize fractured reservoirs: An example from Wyoming: *AAPG Bulletin*, v. 84, p. 830–849.
- Holder, J., J. E. Olson, and Z. Philip, 2001, Experimental determination of subcritical crack growth parameters in sedimentary rock: *Geophysical Research Letters*, v. 28, p. 599–602.
- Hooker, J. H., J. F. W. Gale, L. A. Gomez, S. E. Laubach, R. Marrett, and R. M. Reed, 2009, Aperture-size scaling variations in a low-strain opening-mode fracture set, Cozette Sandstone, Colorado: *Journal of Structural Geology*, v. 31, p. 707–718, doi:10.1016/j.jsg.2009.04.001.
- Jaeger, J. C., and N. G. W. Cook, 1979, *Fundamentals of rock mechanics*: London, Chapman and Hall, 593 p.
- Lander, R. H., R. E. Larese, and L. M. Bonnell, 2008, Toward more accurate quartz cement models—The importance of euhedral vs. non-euhedral growth rates: *AAPG Bulletin*, v. 92, p. 1537–1564, doi:10.1306/07160808037.
- Laubach, S. E., 1988, Subsurface fractures and their relationship to stress history in east Texas Basin sandstone: *Tectonophysics*, v. 156, p. 37–49, doi:10.1016/0040-1951(88)90281-8.
- Laubach, S. E., 1997, A method to detect natural fracture strike in sandstones: *AAPG Bulletin*, v. 81, p. 604–623.
- Laubach, S. E., 2003, Practical approaches to identifying sealed and open fractures: *AAPG Bulletin*, v. 87, p. 561–579, doi:10.1306/11060201106.
- Laubach, S. E., and K. Diaz-Tushman, 2009, Laurentian paleostress trajectories and ephemeral fracture permeability, Cambrian Eriboll Formation sandstones west of the Moine thrust zone, northwest Scotland: *Journal of the Geological Society (London)*, v. 166, p. 349–362, doi:10.1144/0016-76492008-061.
- Laubach, S. E., and J. F. W. Gale, 2006, Obtaining fracture information for low-permeability (tight) gas sandstones from sidewall cores: *Journal of Petroleum Geology*, v. 29, p. 147–158, doi:10.1111/j.1747-5457.2006.00147.x.
- Laubach, S. E., and M. W. Ward, 2006, Diagenesis in porosity evolution of opening-mode fractures, Middle Triassic to Lower Jurassic La Boca Formation, NE Mexico: *Tectonophysics*, v. 419, p. 75–97, doi:10.1016/j.tecto.2006.03.020.
- Laubach, S. E., J. E. Olson, and J. F. W. Gale, 2004a, Are open fractures necessarily aligned with maximum horizontal stress?: *Earth and Planetary Science Letters*, v. 222, p. 191–195.
- Laubach, S. E., R. M. Reed, J. E. Olson, R. H. Lander, and L. M. Bonnell, 2004b, Coevolution of crack-seal texture and fracture porosity in sedimentary rocks: Cathodoluminescence observations of regional fractures: *Journal of Structural Geology*, v. 26, p. 967–982, doi:10.1016/j.jsg.2003.08.019.
- Laubach, S. E., J. E. Olson, and M. R. Gross, 2009, Mechanical and fracture stratigraphy: *AAPG Bulletin*, v. 93, no. 11, p. 1413–1426, doi:10.1306/07270909094.
- Lawn, B. R., and T. R. Wilshaw, 1975, *Fracture of brittle solids*: Cambridge, Cambridge University Press, 204 p.
- Lorenz, J. C., L. W. Teufel, and N. R. Warpinski, 1991, Regional fractures: I. A mechanism for the formation of regional fracture at depth in flat-lying reservoirs: *AAPG Bulletin*, v. 75, p. 1714–1737.
- McLennan, J. A., P. F. Allwardt, P. H. Hennings, and H. E. Farrell, 2009, Multivariate fracture intensity prediction: Application to Oil Mountain anticline, Wyoming: *AAPG Bulletin*, v. 93, no. 11, p. 1585–1595, doi:10.1306/07220909081.
- Miller II, W. K., R. E. Peterson, C. W. Harrison, J. E. Stevens, and C. B. Lackey, 1994, In-situ stress profiling and prediction of hydraulic fracture azimuth for the west Texas Canyon Sands formation: *Society of Petroleum Engineers Production and Facilities*, v. 9, no. 3, p. 204–210.
- Narr, W., and J. B. Currie, 1982, Origin of fracture porosity—Example from Altamont field, Utah: *AAPG Bulletin*, v. 66, p. 1231–1247.
- Narr, W., and J. Suppe, 1991, Joint spacing in sedimentary rocks: *Journal of Structural Geology*, v. 13, p. 1037–1048, doi:10.1016/0191-8141(91)90055-N.
- Nelson, R. A., 1985, *Geologic analysis of naturally fractured reservoirs*: Houston, Texas, Gulf Publishing Co., 320 p.
- Olson, J., and D. D. Pollard, 1989, Inferring paleostresses from natural fracture patterns: A new method: *Geology*, v. 17, p. 345–348, doi:10.1130/0091-7613(1989)017<0345:IPFNFP>2.3.CO;2.
- Olson, J. E., 1993, Joint pattern development: Effects of subcritical crack-growth and mechanical crack interaction: *Journal of Geophysical Research*, v. 98, p. 12,251–12,265, doi:10.1029/93JB00779.
- Olson, J. E., 2003, Sublinear scaling of fracture aperture versus length: An exception or the rule?: *Journal of Geophysical Research*, v. 108, no. B9, p. ETG3-1, Cite ID 2413, doi:10.1029/2001JB000419.
- Olson, J. E., 2004, Predicting fracture swarms—The influence of subcritical crack growth and the crack-tip process zone on joint spacing in rock, in T. Engelder and J. W. Cosgrove, eds., *The initiation, propagation, and arrest of joints and other fractures*: Geological Society (London) Special Publication 231, p. 73–87.
- Olson, J. E., 2007, Fracture aperture, length and pattern geometry development under biaxial loading: A numerical study with applications to natural, cross-jointed systems, in G. Couples and H. Lewis, eds., *Fracture-like damage and localization*: Geological Society (London) Special Publication 289, p. 123–142.

- Olson, J. E., S. E. Laubach, and R. H. Lander, 2007, Combining diagenesis and mechanics to quantify fracture aperture distributions and fracture pattern permeability, *in* L. Lonergan, R. J. H. Jolly, D. J. Sanderson, and K. Rawnsley, eds., *Fractured reservoirs: Geological Society (London) Special Publication 270*, p. 97–112.
- Ortega, O. J., R. Marrett, and S. E. Laubach, 2006, A scale-independent approach to fracture intensity and average fracture spacing: *AAPG Bulletin*, v. 90, p. 193–208, doi:10.1306/08250505059.
- Philip, Z. G., J. W. Jennings, J. E. Olson, S. E. Laubach, and J. Holder, 2005, Modeling coupled fracture-matrix fluid flow in geomechanically simulated fracture networks: *Society of Petroleum Engineers Reservoir Evaluation and Engineering*, v. 8, p. 300–309.
- Pollard, D. D., and A. Aydin, 1988, Progress in understanding jointing over the past century: *Geological Society of America Bulletin*, v. 100, p. 1181–1204.
- Pollard, D. D., P. Segall, and P. T. Delaney, 1982, Formation and interpretation of dilatant echelon cracks: *Geological Society of America Bulletin*, v. 93, p. 1291–1303.
- Prats, M., 1981, Effect of burial history on the subsurface horizontal stresses of formations having different material properties: *Society of Petroleum Engineers Journal*, v. 21, no. 6, p. 658–662.
- Rawnsley, K. D., T. Rives, and J. P. Petit, 1992, Joint development in perturbed stress fields near faults: *Journal of Structural Geology*, v. 14, p. 939–951, doi:10.1016/0191-8141(92)90025-R.
- Rijken, P., 2005, Modeling naturally fractured reservoirs: From experimental rock mechanics to flow simulation: Ph.D. dissertation, University of Texas at Austin, Department of Petroleum and Geosystems Engineering, Austin, Texas, 239 p.
- Rijken, P., J. Holder, J. E. Olson, and S. E. Laubach, 2002, Predicting fracture attributes in the Travis Peak Formation using quantitative mechanical modeling and structural diagenesis: *Transactions of Geological Societies*, v. 52, p. 837–847.
- Salz, L. B., 1977, Relationship between fracture propagation pressure and pore pressure: *Society of Petroleum Engineers Annual Fall Technical Conference and Exhibition*, October 9–12, 1977, Denver, Colorado, SPE Paper 6870, 7 p., doi:10.2118/6870-MS.
- Sayers, C., 2007, Introduction to this special section: *Fractures: The Leading Edge*, v. 26, p. 1102–1105, doi:10.1190/1.2780777.
- Segall, P., 1984, Formation and growth of extensional fracture sets: *Geological Society of America Bulletin*, v. 95, p. 454–462.
- Segall, P., and S. D. Fitzgerald, 1998, A note on induced stress changes in hydrocarbon and geothermal reservoirs: *Tectonophysics*, v. 289, p. 117–128, doi:10.1016/S0040-1951(97)00311-9.
- Segall, P., and D. D. Pollard, 1983, Joint formation in granitic rock of the Sierra Nevada: *Geological Society of America Bulletin*, v. 94, p. 563–575.
- Smart, K. J., D. A. Ferrill, and A. P. Morris, 2009, Impact of inter-layer slip on fracture prediction from geomechanical models of fault-related folds: *AAPG Bulletin*, v. 93, no. 11, p. 1447–1458, doi:10.1306/05110909034.
- Walderhaug, O., 2000, Modeling quartz cementation and porosity loss in Middle Jurassic Brent Group sandstones of the Kvitebjørn field, northern North Sea: *AAPG Bulletin*, v. 84, p. 1325–1339.
- Warpinski, N. R., 1989, Elastic and viscoelastic calculations of stresses in sedimentary basins: *Society of Petroleum Engineers Formation Evaluation*, v. 4, p. 522–530.
- Wu, H., and D. D. Pollard, 2002, Imaging 3-D fracture networks around boreholes: *AAPG Bulletin*, v. 86, p. 593–604.
- Zahm, C. K., and P. H. Hennings, 2009, Complex fracture development related to stratigraphic architecture: Challenges for structural deformation prediction, Tensleep Sandstone at the Alcova anticline, Wyoming: *AAPG Bulletin*, v. 93, no. 11, p. 1427–1446, doi:10.1306/08040909110.
- Zemanek, J., E. E. Glenn, L. J. Norton, and R. L. Caldwell, 1970, Formation evaluation by inspection with borehole televiewer: *Geophysics*, v. 35, p. 254–269, doi:10.1190/1.1440089.
- Zoback, M. D., 2007, *Reservoir geomechanics*: Cambridge, Cambridge University Press, 449 p.
- Zoback, M. D., and J. H. Healy, 1984, Friction, faulting, and in situ stress: *Annales Geophysicae*, v. 2, p. 689–698.
- Zoback, M. D., and J. C. Zinke, 2002, Production-induced normal faulting in the Valhall and Ekofisk oil fields: *Pure and Applied Geophysics*, v. 159, p. 403–420.